NASA/TM—2004-213076 GT2004–53956

Multi-Fidelity Simulation of a Turbofan Engine With Results Zoomed Into Mini-Maps for a Zero-D Cycle Simulation

Mark G. Turner
University of Cincinnati, Cincinnati, Ohio

John A. Reed
AP Solutions, Inc., Solon, Ohio

Robert Ryder
Flow Parametrics, LLC, Ivoryton, Connecticut

Joseph P. Veres
Glenn Research Center, Cleveland, Ohio

November 2004

The NASA STI Program Office . . . in Profile

Since its founding, NASA has been dedicated to the advancement of aeronautics and space science. The NASA Scientific and Technical Information (STI) Program Office plays a key part in helping NASA maintain this important role.

The NASA STI Program Office is operated by Langley Research Center, the Lead Center for NASA's scientific and technical information. The NASA STI Program Office provides access to the NASA STI Database, the largest collection of aeronautical and space science STI in the world. The Program Office is also NASA's institutional mechanism for disseminating the results of its research and development activities. These results are published by NASA in the NASA STI Report Series, which includes the following report types:

- TECHNICAL PUBLICATION. Reports of completed research or a major significant phase of research that present the results of NASA programs and include extensive data or theoretical analysis. Includes compilations of significant scientific and technical data and information deemed to be of continuing reference value. NASA's counterpart of peer-reviewed formal professional papers but has less stringent limitations on manuscript length and extent of graphic presentations.

- TECHNICAL MEMORANDUM. Scientific and technical findings that are preliminary or of specialized interest, e.g., quick release reports, working papers, and bibliographies that contain minimal annotation. Does not contain extensive analysis.

- CONTRACTOR REPORT. Scientific and technical findings by NASA-sponsored contractors and grantees.

- CONFERENCE PUBLICATION. Collected papers from scientific and technical conferences, symposia, seminars, or other meetings sponsored or cosponsored by NASA.

- SPECIAL PUBLICATION. Scientific, technical, or historical information from NASA programs, projects, and missions, often concerned with subjects having substantial public interest.

- TECHNICAL TRANSLATION. English-language translations of foreign scientific and technical material pertinent to NASA's mission.

Specialized services that complement the STI Program Office's diverse offerings include creating custom thesauri, building customized databases, organizing and publishing research results . . . even providing videos.

For more information about the NASA STI Program Office, see the following:

- Access the NASA STI Program Home Page at ***http://www.sti.nasa.gov***

- E-mail your question via the Internet to help@sti.nasa.gov

- Fax your question to the NASA Access Help Desk at 301–621–0134

- Telephone the NASA Access Help Desk at 301–621–0390

- Write to:
  NASA Access Help Desk
  NASA Center for AeroSpace Information
  7121 Standard Drive
  Hanover, MD 21076

NASA/TM—2004-213076 GT2004–53956

Multi-Fidelity Simulation of a Turbofan Engine With Results Zoomed Into Mini-Maps for a Zero-D Cycle Simulation

Mark G. Turner
University of Cincinnati, Cincinnati, Ohio

John A. Reed
AP Solutions, Inc., Solon, Ohio

Robert Ryder
Flow Parametrics, LLC, Ivoryton, Connecticut

Jospeh P. Veres
Glenn Research Center, Cleveland, Ohio

Prepared for the
Turbo Expo 2004
sponsored by the American Society of Mechanical Engineers
Vienna, Austria, June 14–17, 2004

National Aeronautics and
Space Administration

Glenn Research Center

November 2004

Acknowledgments

The authors would like to thank Andrew Norris, Scott Towsend, Jim Felder, Bill Pavlik, Jeff Moder, Nan-Suey Liu, John Adamczyk, John Lytle, Lonnie Reid, Greg Follen, and the members of the NPSS development team for their help in this research. Special thanks to Ron Plybon at General Electric for his assistance. The work described in this paper was supported by the NASA Ultra-Efficient Engine Technology (UEET) and NASA Aerospace Propulsion and Power programs.

This report contains preliminary findings, subject to revision as analysis proceeds.

This work was sponsored by the Low Emissions Alternative Power Project of the Vehicle Systems Program at the NASA Glenn Research Center.

Available from

NASA Center for Aerospace Information
7121 Standard Drive
Hanover, MD 21076

National Technical Information Service
5285 Port Royal Road
Springfield, VA 22100

Available electronically at http://gltrs.grc.nasa.gov

Multi-Fidelity Simulation of a Turbofan Engine with Results Zoomed into Mini-Maps for a Zero-D Cycle Simulation

Mark G. Turner
University of Cincinnati
Cincinnati, Ohio 45221

John A. Reed
AP Solutions, Inc.
Solon, Ohio 44139

Robert Ryder
Flow Parametrics, LLC
Ivoryton, Connecticut 06442

Joseph P. Veres
National Aeronautics and Space Administration
Glenn Research Center
Cleveland, Ohio 44135

ABSTRACT

A Zero-D cycle simulation of the GE90-94B high bypass turbofan engine has been achieved utilizing mini-maps generated from a high-fidelity simulation. The simulation utilizes the Numerical Propulsion System Simulation (NPSS) thermodynamic cycle modeling system coupled to a high-fidelity full-engine model represented by a set of coupled 3D computational fluid dynamic (CFD) component models. Boundary conditions from the balanced, steady-state cycle model are used to define component boundary conditions in the full-engine model. Operating characteristics of the 3D component models are integrated into the cycle model via partial performance maps generated from the CFD flow solutions using one-dimensional meanline turbomachinery programs. This paper highlights the generation of the high-pressure compressor, booster, and fan partial performance maps, as well as turbine maps for the high pressure and low pressure turbine. These are actually "mini-maps" in the sense that they are developed only for a narrow operating range of the component. Results are compared between actual cycle data at a take-off condition and the comparable condition utilizing these mini-maps. The mini-maps are also presented with comparison to actual component data where possible.

NOMENCLATURE

A_z	annular area
h	enthalpy
P	pressure
r	radius
R	gas constant
T	temperature
h	enthalpy
P	pressure
V	velocity
$\dot{m}$	mass flow rate
ρ	density
ω	shaft rotational speed
γ	specific heat ratio

Subscripts:

h	hub
t	tip
T	total or stagnation conditions
_	tangential
z	axial

Superscripts:

=	mass-averaged

INTRODUCTION

This paper presents recent work on a full engine simulation that is part of a broader effort that has been under development at NASA Glenn Research Center for some time. A detailed account of the background of this effort was presented by Reed et al. [1]. A brief account of the background is described in this section as well as a layout of the rest of the paper.

The NASA Glenn Research Center is developing the capability to decrease aerospace product development time through the use of computational simulation technology known as Numerical Propulsion System Simulation (NPSS). NPSS will be capable of analyzing a propulsion system in sufficient detail to resolve effects of multidisciplinary processes and component interactions currently only observable in large-scale tests as described by Lytle [2, 3].

Historically, the design of an aircraft engine begins with a study of the complete engine using a relatively simple aerothermodynamic "cycle" analysis. The operating characteristics of the engine's components (fan, compressor, turbine, etc.) are represented in the study by performance maps, which are based on experimental test data of existing components. As the process continues, component designs are refined until component and engine performance goals are met.

Component design teams rely on advanced numerical techniques to understand component operation and achieve the best performance. Streamline curvature methods as described by Smith [4] and Adkins and Smith [5] calculate flow properties on multiple streamlines across the component's span, and are still widely used in turbomachinery design and analysis. More recently, improvements in the speed and availability of computer processors have enabled advanced 3D numerical techniques to be applied to the design of isolated components. Methods for simulating multistage turbomachinery have also been developed, and are now being applied in the design process as described by Adamczyk [6] and Hall [7, 8].

It is important to consider the engine as a system of components which influence each other, and not simply as isolated components. A high-fidelity full-engine simulation can provide more details about component interactions than using performance maps alone. Toward that end, the present work was undertaken to extend engine simulation capability from isolated components to the full engine, by integrating advanced component simulations to form a full, 3D turbofan engine simulation.

The detailed simulation of a complete aircraft engine requires considerable computing capacity. To be an effective design tool, the wall-clock execution times for a full engine simulation must be reduced to the point where it can impact the design process. This translates into approximately 15 hours so that the simulation may be run overnight. In addition to high-performance computing capabilities, improved modeling techniques are necessary to reduce the computing requirements for detailed simulation of the entire engine. One technique is variable complexity analysis, often referred to as "zooming" in NPSS publications by Follen and auBuchon [9] and Hall et al. [10], allows a designer to vary the level of detail of analysis throughout the engine based upon the physical processes being studied.

In this paper, the progress made towards demonstrating a 3D aerodynamic simulation of a complete turbofan engine is described. The simulation is comprised of coupled 3D, computational fluid dynamics (CFD) component simulations for both the core and bypass flow paths. A form of variable complexity analysis (zooming and unzooming) is used to reduce setup and simulation times for the 3D analysis by coupling a cycle model to the 3D model. The cycle model uses partial performance maps ("mini-maps") to obtain a balanced steady-state engine condition. The balanced cycle model then provides boundary conditions, such as flows and wheel speeds, to run the complete 3D engine simulation. The mini-maps are generated from 1D meanline programs whose input data is obtained from the unzoomed 3D component's flow solutions.

The rest of the paper includes the methodology used including the mini-map generation, the full engine simulation process, results, conclusions and future work.

METHODOLOGY

The GE90-94B turbofan engine, a production engine offered on the Boeing 777-200ER aircraft, was used in this demonstration (see Fig. 1). A sea-level, Mach 0.25, take-off condition was selected for the simulation. The main reason for this selection was that cooling flows for the turbine represent a significant amount of boundary condition information for the simulation, and these are best known at take-off. This represents the heat transfer design point, and also represents a condition where there are the highest temperatures and most stress in the engine.

The fan is 120 inches in diameter and consists of 22 composite wide-chord blades. The fan outlet guide vane (OGV) has several types with differing camber; only the nominal type is modeled in the simulation. The booster consists of 3 stages (7 blade rows). A frame strut separates the booster and HPC,

Figure 1. GE90 Engine

which consists of 10 stages (21 blade rows). The combustor is a dual dome annular design consisting of 30 pairs of fuel nozzles around the annulus. Due to periodicity of the geometry, only 2 pairs of the fuel nozzles (a 24-degree sector) need be modeled. The 2-stage (4 blade rows) high pressure turbine (HPT), the mid-frame strut, and the 6-stage (12 blade rows) low pressure turbine (LPT) are modeled as a single component.

The full-turbofan engine simulation utilizes the NPSS thermodynamic cycle system modeling software described by Evans et al. [11], along with toolkits developed for NPSS, to couple the high-fidelity 3D CFD software. NPSS is a component-based, object-oriented, engine cycle simulator designed to perform cycle design, steady state and transient off-design performance prediction.

An NPSS engine model is assembled from a collection of interconnected elements and sub-elements, and controlled by an appropriate numerical solver. The model is defined using the NPSS programming language, and executed in interpreted or compiled form by the NPSS software. For the GE90-94B, the NPSS model consists of forty-three elements representing the primary and secondary bleed flow, shaft and control system components. The input data for the model was obtained from a General Electric cycle model of the GE90-94B at the take-off conditions described above. This GE data was also used to verify and validate the NPSS cycle model.

The high-fidelity full-engine model consists of 3D CFD models of the fan, booster, high-pressure compressor (HPC), combustor, and full turbine comprising both the high-pressure turbine (HPT) and low-pressure turbine (LPT). The combustor model is simulated using the National Combustor Code (NCC) combustor model described by Liu and Quealy [12], Liu [13], Ryder and McDivitt [14] and Ebrahimi et al. [15]. The turbomachinery component models are simulated using APNASA described by Adamczyk et al. [16] and Kirtley et al. [17]. These component blocks are shown in Fig. 2. All turbomachinery component simulations have been analyzed and compared with GE90 component test data to validate and calibrate the simulation. These efforts have been presented by Turner [18], Turner et al. [19], and Adamczyk [6]. Figure 3 shows the 3D features in HPC rotor 6 that are only a small feature in this large complex simulation.

NCC is a parallel-unstructured solver that uses a preconditioner to efficiently handle low Mach number flows. The Navier-Stokes equations are solved using an explicit four-stage Runge-Kutta scheme. Turbulence closure is obtained via the standard k-ε model with a high Reynolds number wall function, or a non-linear k-ε model for swirling flows. NCC can be run with different fuel models and combustion models. Figures 4, 5 and 6 show the geometry, grid and total temperature contours from the NCC simulation.

The average passage approach of Adamczyk et al. [16] is incorporated into the APNASA program. The foundation of the APNASA Navier-Stokes solver is an explicit four-stage Runge-Kutta scheme with local time-stepping and implicit residual smoothing to accelerate convergence. Second and fourth difference smoothing as applied by Jameson and Baker [20] is employed for stability and shock capturing. A k-ε turbulence model is solved using an implicit upwind approach similar to that presented by Turner and Jennions [21] and Shabbir et. al. [22]. Wall functions are employed to model the turbulent shear stress adjacent to the wall without the need to resolve the entire boundary layer.

Mini-map Generation

As described in the introduction, performance characteristics of the 3D CFD components are represented in the cycle simulation by partial performance maps. These "mini-maps" define component operating characteristics over a small operating range around some desired point. They provide a physics-based estimate of component performance and replace the default maps within the NPSS cycle model.

Because it takes a large amount of computational time to converge the CFD simulations and the convergence levels would have to be very tight to eliminate noise in a CFD generated mini-map, a strategy has been implemented to utilize only one CFD simulation of a component to generate the mini-map.

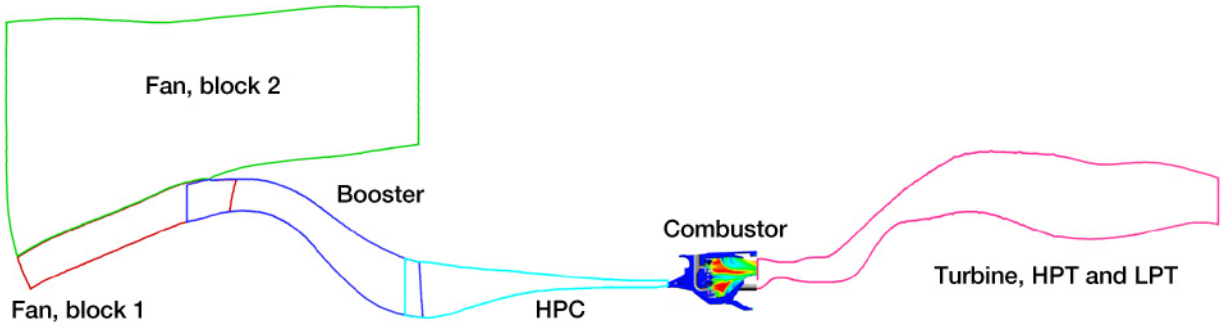

Figure 2. Five domains simulated in sequence inlet to exit

Circumferentially averaged quantities are extracted from the 3D multistage simulations and used as input to 1-D meanline programs. This has been demonstrated for the HPC and presented by Reed et al. [1]. The APNASA flow solution is averaged to obtain input for the 1D meanline stage-stacking program (STGSTK) described by Steinke [23], which generates a compressor mini-map. Pressure ratio and efficiency are input for each stage along with the absolute flow angle at the mean line into each rotor. Hub and casing radii are needed at each station. The rotor and stator leading edge angles at the meanline are used to define the incidence angles which are used along with solidity in an efficiency loss correlation. The main assumption in STGSTK is that the maximum efficiency at each stage is defined by the input data, which is assumed to be the design point. Because the input comes from an APNASA simulation at the operating point it was run at, that will most likely not be the maximum efficiency point.

Currently, the fan, booster and HPC are using the STGSTK generated mini-maps from the 3D simulation. The HPT and LPT mini-maps have used a different approach, the details of which will be described in a future paper. An entropy-based 1D blade row model has been developed for turbines written using the NPSS programming language. This allows many features of the 1D model to be entirely consistent with the zero-D or cycle, including the thermodynamics and cooling flows. At this point there is no automatic coupling, and the cooling flows are not yet perfectly consistent. The HPT has a significant amount of cooling flows added in the blade row. This has been modeled in the blade row code as a constant pressure mixing process with the cooling flow added at the upstream interface of the blade row. The entropy generation due to mixing is bookkept separately. The entropy rise due to losses is defined as a bladerow entropy loss coefficient as defined by Denton [24]. For the mini-map generation, this loss coefficient is kept constant for the other flow conditions. The LPT model has added hub seals for nozzles and casing seals for the rotors to represent the shrouded blades. The continuity, angular momentum, and energy equations are satisfied across each blade row. An entropy equation is applied which accounts for mixing loss and other loss mechanisms. The unshrouded rotor in the HPT has an extra term in the energy equation that is calculated in the high fidelity simulation and described by Lyman [25].

In order to be as consistent as possible between the high fidelity APNASA simulation and the STGSTK and turbine 1D models, the circumferential averaging has been defined consistently. Stations between the blade rows or at leading and trailing edges are used to define the hub and casing radii. This same station is post-processed in the 3-D simulation. The mass-averaged values of total pressure $\overline{\overline{P_T}}$, total enthalpy $\overline{\overline{H_T}}$, and angular momentum $\overline{\overline{rV_\theta}}$ are evaluated. The mass flow rate ($\dot{m}$) and the annular area (A_z) are also needed. The annular area comes from the hub and tip radii (r_h and r_t). Quantities with an under-bar are derived.

$$A_z = \pi(r_t^2 - r_h^2) \tag{1}$$

$$r_m \equiv \sqrt{r_t^2 - \frac{A_z}{2\pi}} \tag{2}$$

$$V_\theta \equiv \frac{\overline{\overline{rV_\theta}}}{r_m} \tag{3}$$

$$\underline{\rho V_z} \equiv \frac{\dot{m}}{A_z} \tag{4}$$

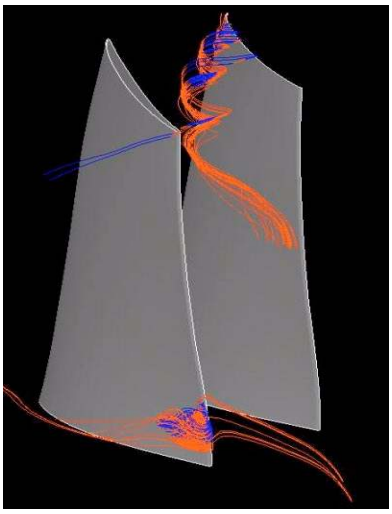

Figure 3. Streamlines in HPC Rotor 6 showing tip vortex and hub corner separation.

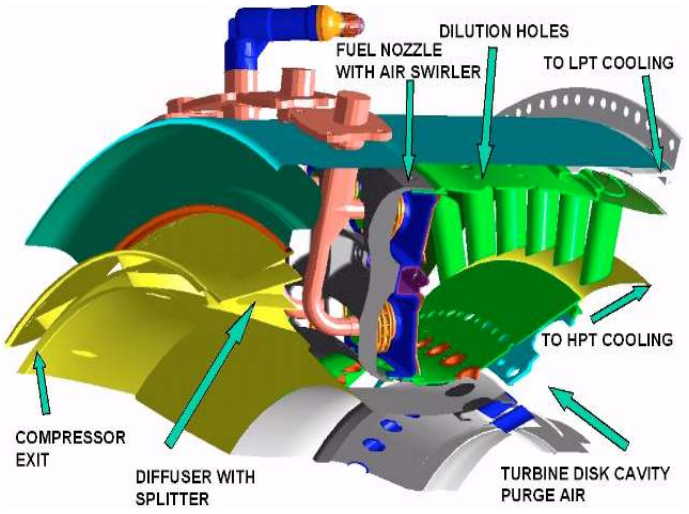

Figure 4. Geometry of the GE90 Combustor

$$V = \sqrt{V_z^2 + V_\theta^2} \tag{5}$$

where the radial component of velocity is ignored in STGSTK and this analysis.

$$h = \overline{\overline{H_T}} - \frac{V^2}{2} \tag{6}$$

T and T_T come from h and $\overline{\overline{H_T}}$, and the enthalpy-temperature relation used in APNASA.

$$P = P_T\left(\frac{T}{T_T}\right)^{\frac{\gamma}{(\gamma-1)}} \tag{7}$$

$$\rho = \frac{P}{RT} \tag{8}$$

$$V_z = \frac{\rho V_z}{\overline{\overline{\rho}}} \tag{9}$$

Equations (5)-(9) are iterated to convergence.

$$W_\theta = V_\theta - r_m\omega \tag{10}$$

$$\alpha = \text{atan}\left(\frac{V_\theta}{V_z}\right) \tag{11}$$

$$\beta = \text{atan}\left(\frac{W_\theta}{V_z}\right) \tag{12}$$

This equation system is evaluated at each station, and the meanline flow angles are input into STGSTK or the 1D turbine meanline code.

Full Engine Simulation Process

The full-engine simulation has followed the following process:

1. Started using the GE GE90-94B cycle point.
2. All turbomachinery components were run and compared to GE90 component test data to validate and calibrate the simulations. These efforts have been presented by Turner [18], Turner et al. [19], and Adamczyk [6].
3. The combustor was run and compared to expected profiles and pressure drop for this configuration.
4. The core was run by coupling the HPC, Combustor and Turbine in an upstream to downstream sequence. This effort was reported by Turner et al. [26].
5. The high-fidelity full engine simulation was run in an upstream to downstream sequence starting at the inlet. Shaft speeds were set by the GE cycle model. The BCs are applied to each 3D model through the APNASA and NCC input files. The loosely-coupled CFD engine component simulations exchange radial profile boundary conditions at the inlet and exit plane of each adjacent component. Script files on the SGI Origin submit runs to the Portable Batch System [27] to execute the programs, and manipulate files (such as "fliping" the APNASA output files). The APNASA program, using mesh files and other input files, generates a set of flow solution files. The APNASA Circumferential Averaging Tool, APNASACAT, uses these files to generate the 2-D averaged flow solution. This data is then used to generate the inlet profile for the downstream component. Special processing is required between the HPC and combustor due to differences in modeling methodologies between APNASA and NCC, and another averaging tool is used to extract the profiles from NCC and pass

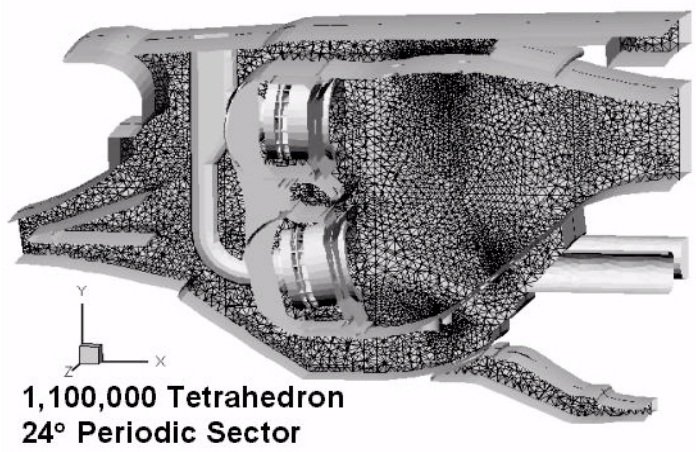

Figure 5. Unstructured grid of the GE90 Combustor used by NCC.

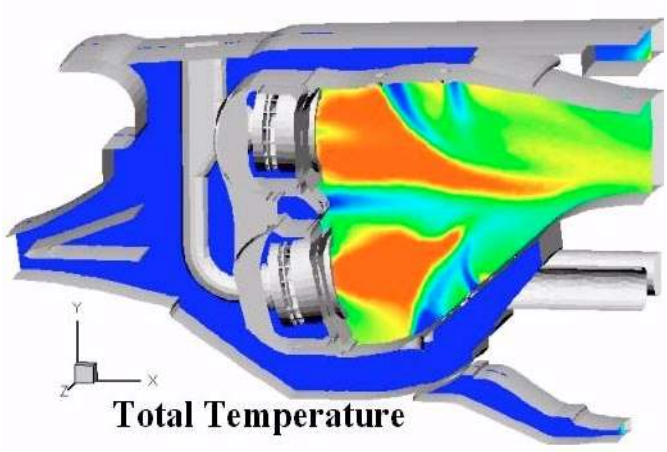

Figure 6. Combustor Simulation

them onto the HPT. Figure 7 shows the balance of properties and their deviation from the GE cycle after proceeding from inlet to exit. The "numerical machine" did not operate exactly at the cycle condition. The torque balance for each shaft is shown in Fig. 8 for this initial simulation. Much of this effort has been presented by Turner et al. [28].

6. The NPSS cycle model of the GE90-94B has been developed, tested and verified against the GE cycle. In a comparison of 131 key cycle parameters, the NPSS model deviated no more than 0.5% from the GE baseline data, with a majority of the parameters deviating less than 0.01% from the baseline. Figure 9 is a schematic of the cycle model.

7. The 3D turbomachinery component simulations are averaged using the APNASACAT code to supply information to STGSTK or the turbine meanline code. Mini-maps for the component are generated. These maps will be presented in the Results section. Special processing is done for the fan and booster to duplicate the model used in the cycle. This model assumes the splitter is upstream of the fan and the lower part of the fan is part of the booster component. The fan has been run in APNASA with a multi-block approach. The inner block is assumed to be only core flow and part of the booster. The outer block is part of the bypass.

8. The NPSS cycle of the full engine is run using the mini-maps for the fan, booster, HPC, HPT and LPT. The duct losses for the strut following the booster, the strut following the HPT and the OGV following the LPT are also obtained and used from the CFD simulation. The combustor 3D model at this point has not been used. That is because the combustor efficiency and pressure drop numbers compare well and the comparison at this point is with the turbomachinery only. It should be emphasized that the mini-maps have been used as they come from the 1D blade row codes. The only manipulation is to get them in the right tabular format used by NPSS. A comparison is presented in the Results section between the cycle information from NPSS calibrated to the GE cycle (design) and the NPSS simulation using the mini-maps and duct losses from the 3D CFD (off-design).

The process defined by items 5-8 is illustrated in Fig. 10.

RESULTS

The GE90 has its roots in the NASA/GE EEE engine development program which led to component tests in the early 1980's. The first production GE90 HPC was a direct scale of the EEE HPC that is discussed in a GE contractor report to NASA [29]. The GE90-94B HPC is an improved version of that. For comparison purposes, the EEE HPC map is plotted in Fig. 11.

The component mini-maps have been calculated with the 1D blade row codes. They are plotted in Figs. 12-16 for the fan, booster, HPC, HPT and LPT. The STGSTK approach was used for the fan, booster and HPC. The entropy-based blade row model using NPSS was used for the HPT and LPT. On each plot are the speed lines calculated by the blade row codes and 3 points. They are labeled as:

1. Cycle, Take-Off which is the NPSS cycle run based on the GE cycle,

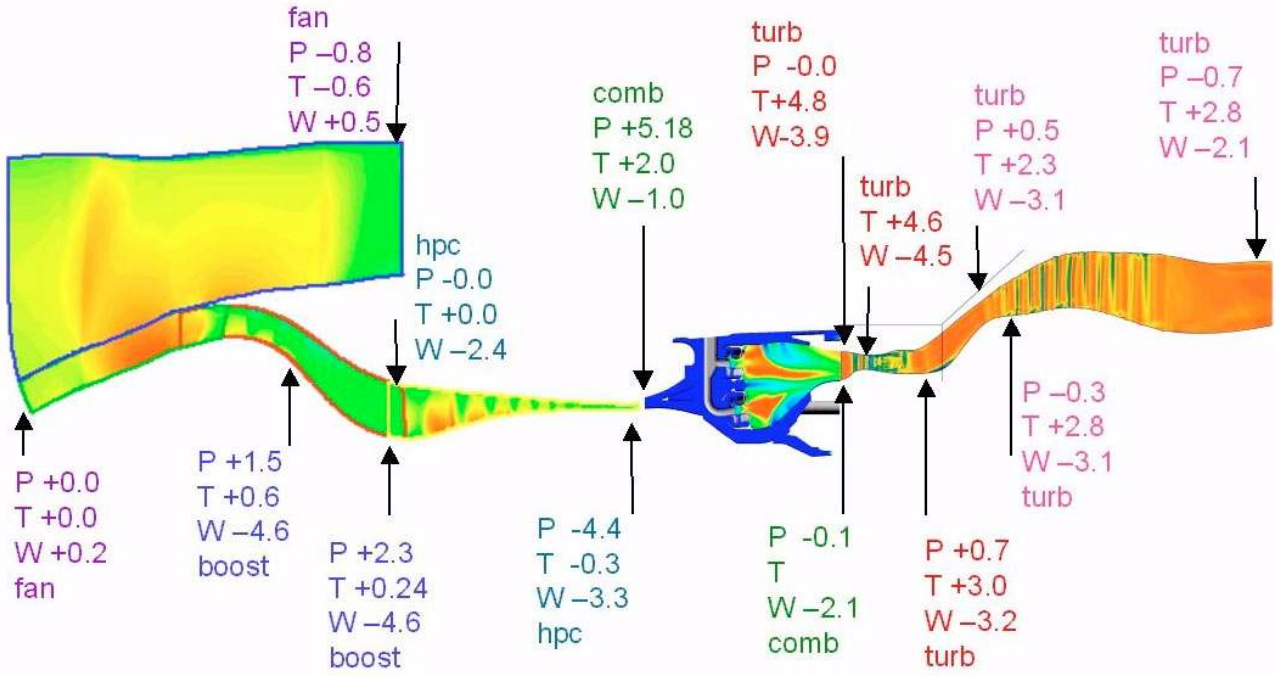

Figure 7. Full engine simulation comparison to cycle. Percent difference in Total Pressure (P), Total Temperature (T) and FlowRate (W).

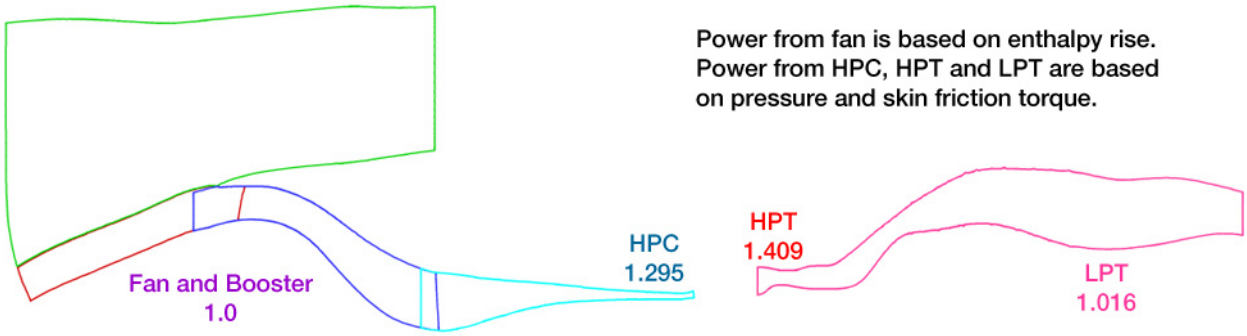

Figure 8. Power Balance. Power normalized by Fan and Booster. Power to pump cooling flows not subtracted from HPT. Work by HPC under-predicted.

2. CFD which is the condition the CFD 3D simulation ran to after running the upstream to downstream sequence, and
3. Cycle, w/Mini-maps which is the result of running NPSS using the mini-maps and CFD derived duct losses.

These maps will be discussed further below.

A comparison is given in Table I between the Cycle run based on the GE cycle (design) and the Cycle with mini-maps (off-design). These two cycle simulations held the specified fuel flow constant. It must be recalled that the mini-maps have been used as is without any scale factors or adders. The total temperature at the LPT exit, or EGT is 1.6 degrees C higher for the Cycle with mini-maps. Plybon [30] suggests a representative new engine-to-engine variation for the purpose of comparing a fully predictive code to engine data and limiting expectations on the level of agreement are plus or minus 4 degrees C EGT (LPT exit), 0.25% SFC, or 0.5% Thrust.

Table 1 shows the difference in efficiency, and relative difference in corrected flow, pressure ratio and corrected speed for each component for both the Cycle based on the GE cycle and the Cycle using mini-maps. The corrected-speeds, as well as both mechanical shafts speeds, are about 1% higher for the Cycle with mini-maps than the GE based cycle. The relative difference in Specific Fuel Consumption (SFC), Bypass Ratio (BPR) and Overall Pressure Ratio (OPR) are also tabulated. The relative difference of SFC is almost 1% lower for the Cycle with mini-maps. The EGT difference is smaller than an engine-to-engine variation, although the SFC is not.

The mini-maps shown in Figs. 12-16 plot corrected flow, pressure ratio and efficiency. By comparing with Table I the scale of the plots can be inferred. It is apparent that these maps are only for a small region of the component characteristic. It can also be seen how the efficiencies are the main difference between the CFD components and the GE cycle. There are three known issues. One is that the CFD assumes turbulent flow everywhere. This is probably not the case for part of the LPT, and is probably why the LPT efficiency is low in the cycle with mini-maps. This is also most likely why the corrected flow is low for the LPT from the mini-maps. The comparison of the APNASA solutions compared to rig data show a similar trend for flow as reported by Turner et al. [19] with the HPT 2.5% high and the LPT 2.5% low relative to rig data. Other CFD modeling discrepancies also play a role, such as fan OGV differences might have the CFD efficiencies higher for the fan than actual. The other issue is that the loss models are crude in the 1D blade row models. In the STGSTK approach, the "design" value is set to the highest efficiency. For the entropy-based approach, the blade row entropy loss coefficient is treated as a constant. This is not necessarily the case, especially if running low in flow. Future work will address improvements in the loss models.

This cycle with mini-map simulation is good although improvements can be made. It must be remembered that it is based solely on numerical simulation of an engine that consists of 49 blade rows of turbomachinery. The combustor model in the cycle with mini-maps is consistent in overall parameters with the CFD simulation. This is therefore the first engine simulation with power balance to be entirely run based on numerical simulation.

CONCLUSIONS AND FUTURE WORK

A Zero-D cycle simulation of the GE90-94B high bypass turbofan engine has been achieved utilizing mini-maps generated from a high-fidelity simulation.

Three dimensional CFD simulations of the fan, booster, HPC, HPT and LPT have been performed using the APNASA turbomachinery code. The combustor flow and chemistry were simulated using the National Combustor Code, NCC. A cycle model of the engine was developed and verified, and used to provide boundary conditions to the 3D CFD component simulations for the 0.25 Mach, sea-level take-off condition.

Two methods have been presented for generating partial performance maps or mini-maps by appropriate averaging of the 3D CFD flow solutions for use in a 1-D meanline program. The

first method for the compression components utilize the stage-stacking program, STGSTK. The Fan, booster, and HPC mini-maps were generated with this approach. The second method uses an entropy-based blade-row model for turbines written using NPSS. This allows thermodynamics and cooling flow to be consistent between the cycle (zero-D) and 1D models. The LPT has seal models to simulate the shrouded nozzles and rotors. The HPT and LPT mini-maps were generated this way.

The mini-maps of the turbomachinery components and the CFD generated duct losses have been used to run the NPSS cycle model of the GE90-94B engine. The mini-maps were used as is, with no adders or scaling. A comparison of the NPSS model calibrated using the GE cycle model of the engine and the NPSS model using the mini-maps has been made. The comparison shows that the fan and HPT CFD solutions are at a higher efficiency than the GE model, whereas each other component using the CFD-1D model-generated mini-maps is lower in efficiency than the GE model. This difference in efficiency causes the engine to operate at a 1% higher wheel speed in both the low pressure spool and core. The EGT difference between the models is 1.6 degrees C which is smaller than new engine-to-engine differences.

Although the agreement can improve, it is good and this simulation represents the first time a full engine simulation, including the power balance, has been achieved through computational simulation alone. This is also a useful demonstration of the full power of multi-fidelity simulation utilizing zooming and unzooming. By integrating the cycle modeling and high-fidelity simulations, both approaches will be improved. Several areas have also been identified to improve the simulation. The loss models in the 1D blade row codes used to create the mini-map are very crude, and will restrict the efficiency to a low value based on the 3D component simulation. Better consistency between bleed flows and cooling flows must also be achieved.

The next step in this research is to run the full simulation to reach a power-balance in the 3D CFD engine model. One aspect of the simulation we expect to address at that point will be consistency between the CFD and cycle models, especially with addressing the thermodynamic inconsistencies between APNASA, NCC and NPSS. With consistent models it is expected that the whole system will close. Other issues such as techniques for modeling bleeds and cooling flows must also be addressed. One way to address consistency better will be to

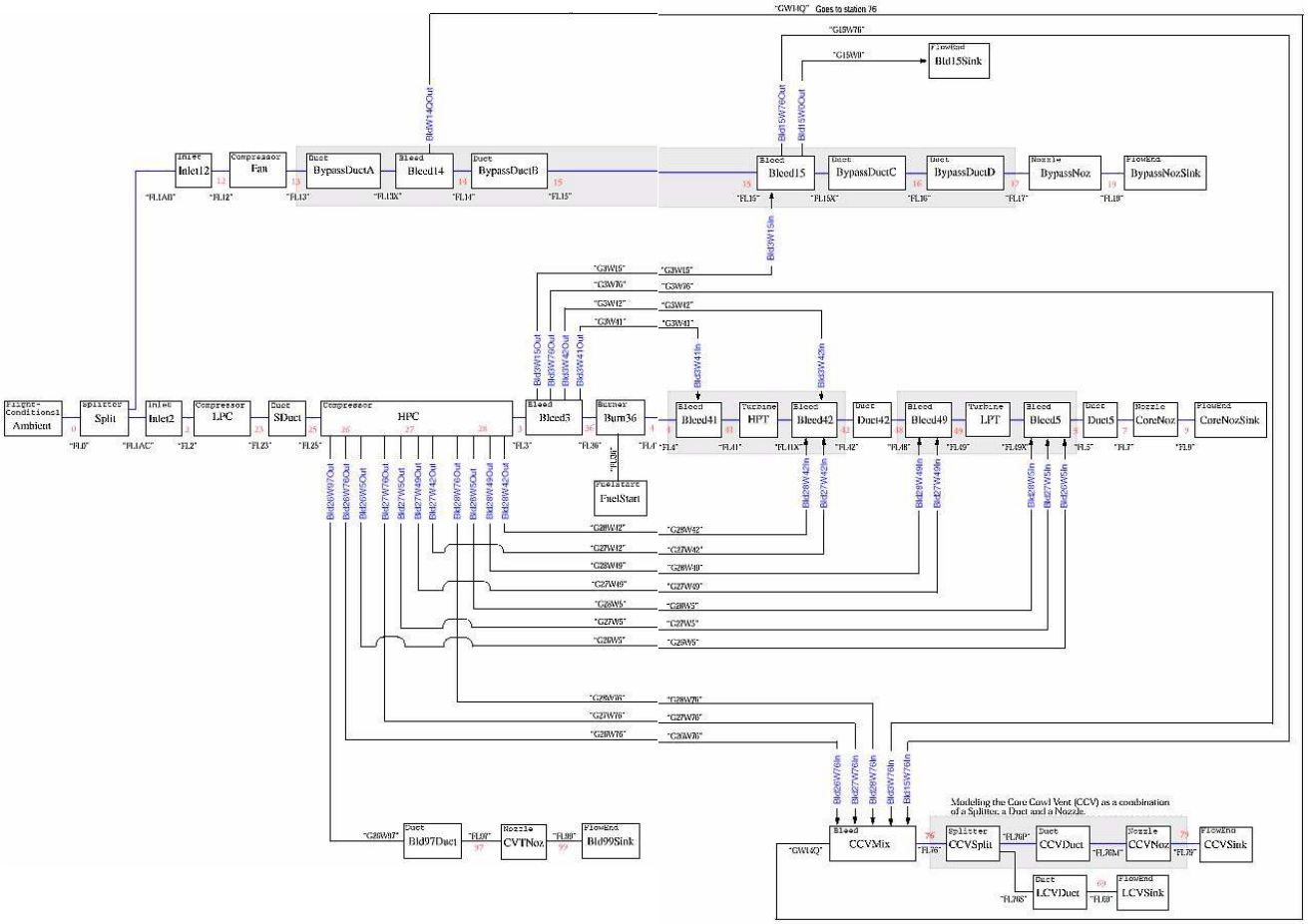

Figure 9. GE90 cycle schematic.

Table 1: Comparison of Cycle simulation at takeoff. Design is based on NPSS run with GE Cycle; Off-design is based on NPSS run with mini-maps. In each case the fuel flow was held fixed. Efficiency is quoted at Off-design - Design. Other quantities are Relative Differences of (Off-design - Design)/Design.

	Wc (rel diff)	PR (rel diff)	TR (rel diff)	η_{ad} (% diff)	Nc (rel diff)
Fan	0.71%	0.45%	-0.17%	2.32%	1.09%
Booster	0.08%	-0.60%	0.08%	-1.37%	1.09%
HPC	0.75%	-0.49%	0.05%	-0.29%	0.97%
HPT	1.21%	-3.52%	0.06%	1.79%	0.99%
LPT	-2.34%	2.35%	-0.22%	-1.54%	1.00%
	SFC	**BPR**	**OPR**		
Relative Difference	-0.99%	0.63%	-1.10%		

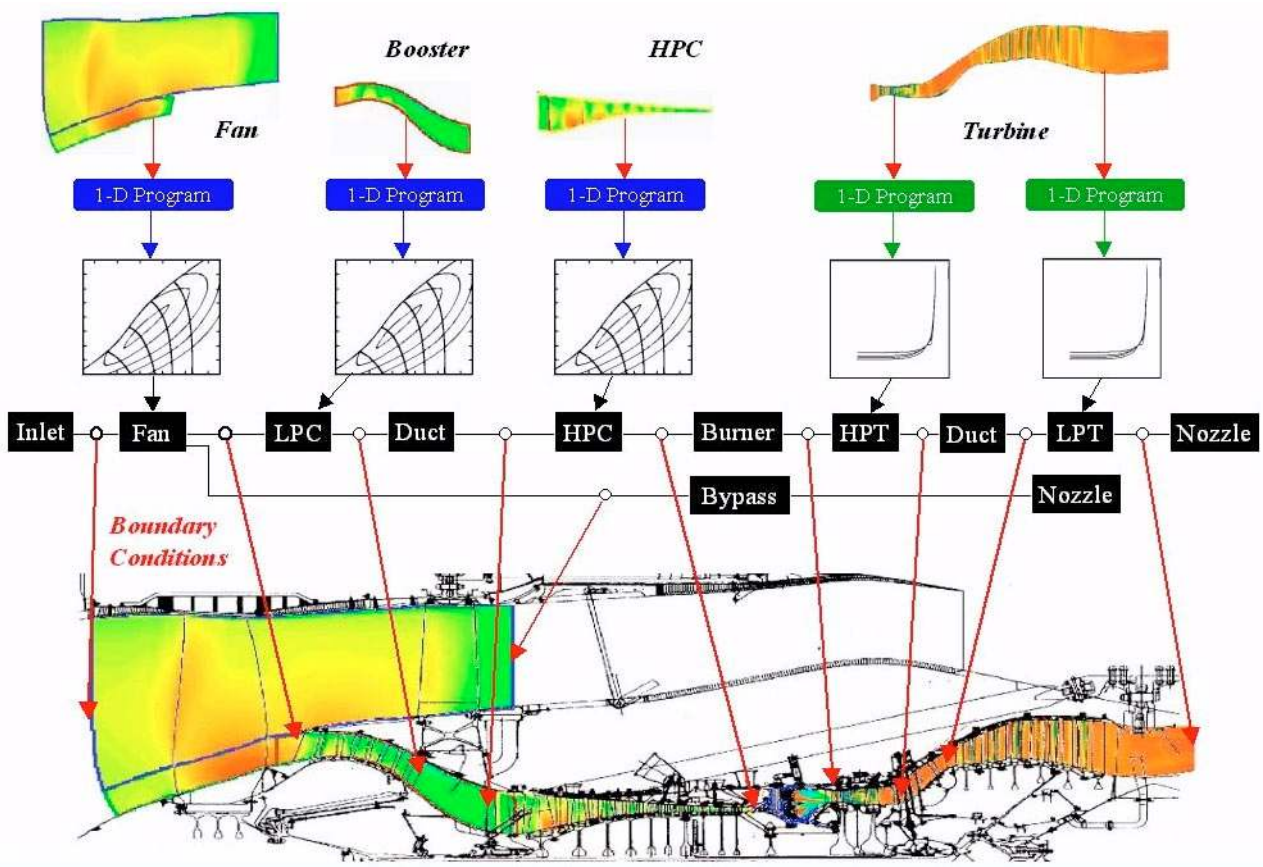

Figure 10. Coupling of 3-D full engine model with 0- D cycle model. From bottom to top: 3-D CFD component model flow solutions are automatically used by 1-D meanline programs to generate mini-maps. Maps are included in appropriate components in GE90 cycle model. Converged cycle boundary conditions are used to set boundary conditions in CFD components for coupled full-engine simulation. Top of figure shows axisymmetric plot of absolute Mach number overlayed on GE90 engine geometry.

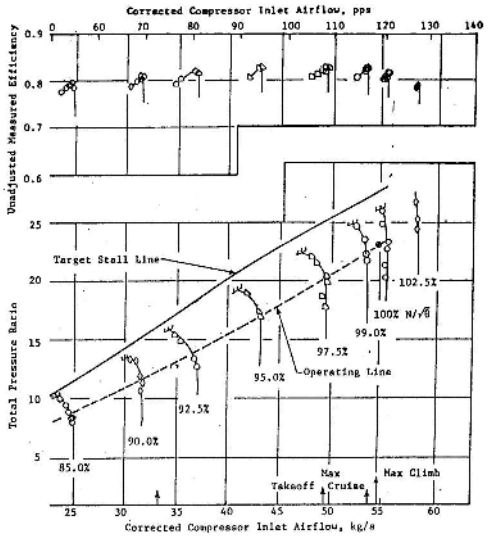

Figure 11. Energy Efficient Engine (EEE) high-pressure compressor map (see ref. 31 for similar map).

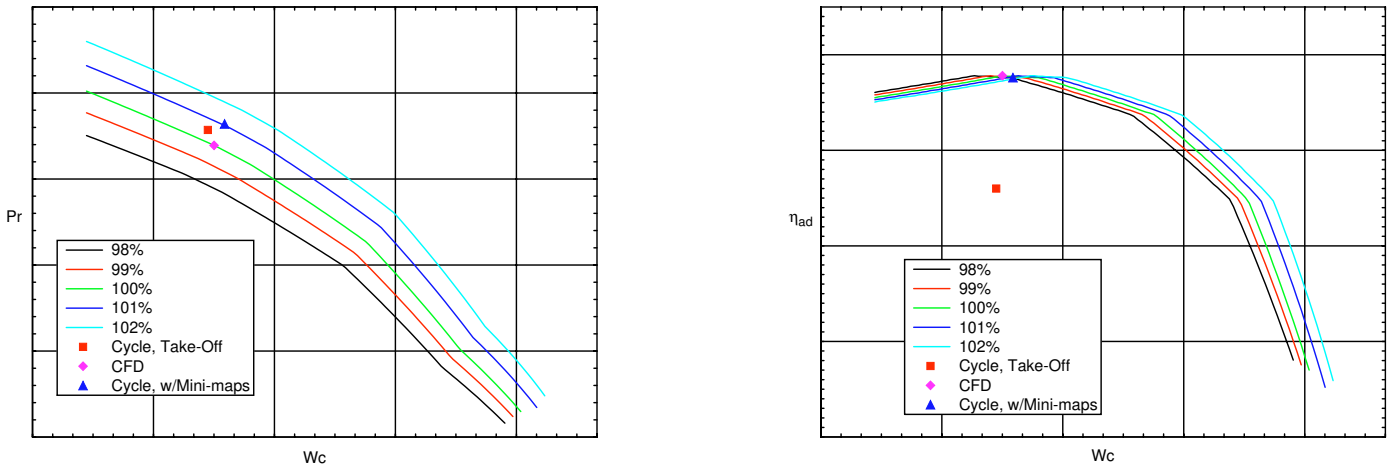

Figure 12. Fan mini-maps. Pressure-ratio (PR) and adiabatic efficiency (η_{ad}) as function of corrected mass flow rate (Wc) for a set of speed lines.

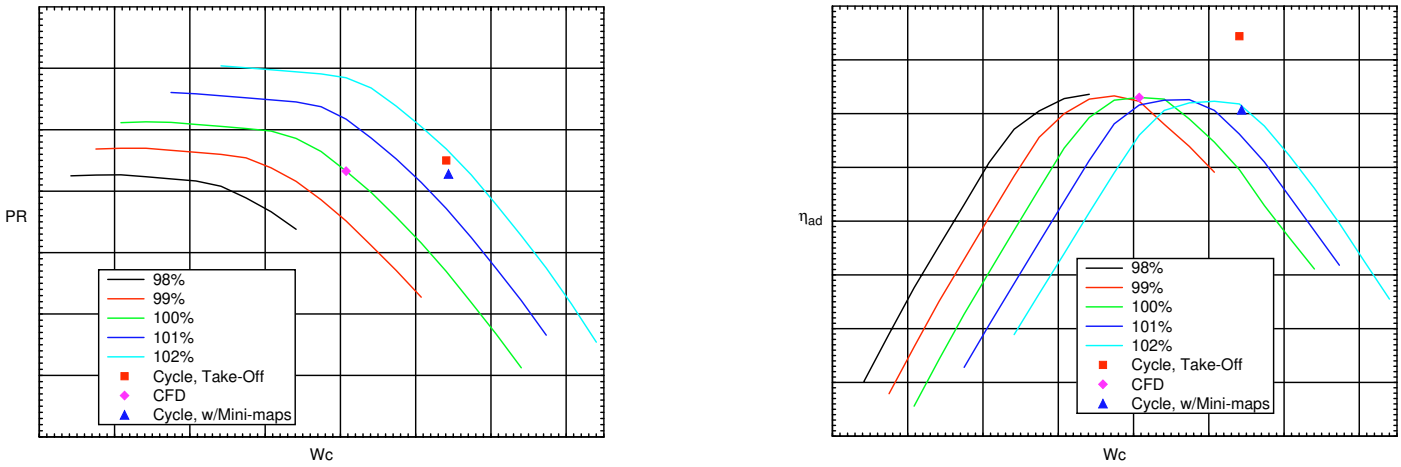

Figure 13. Booster mini-maps. Pressure-ratio (PR) and adiabatic efficiency (η_{ad}) as function of corrected mass flow rate (Wc) for a set of speed lines.

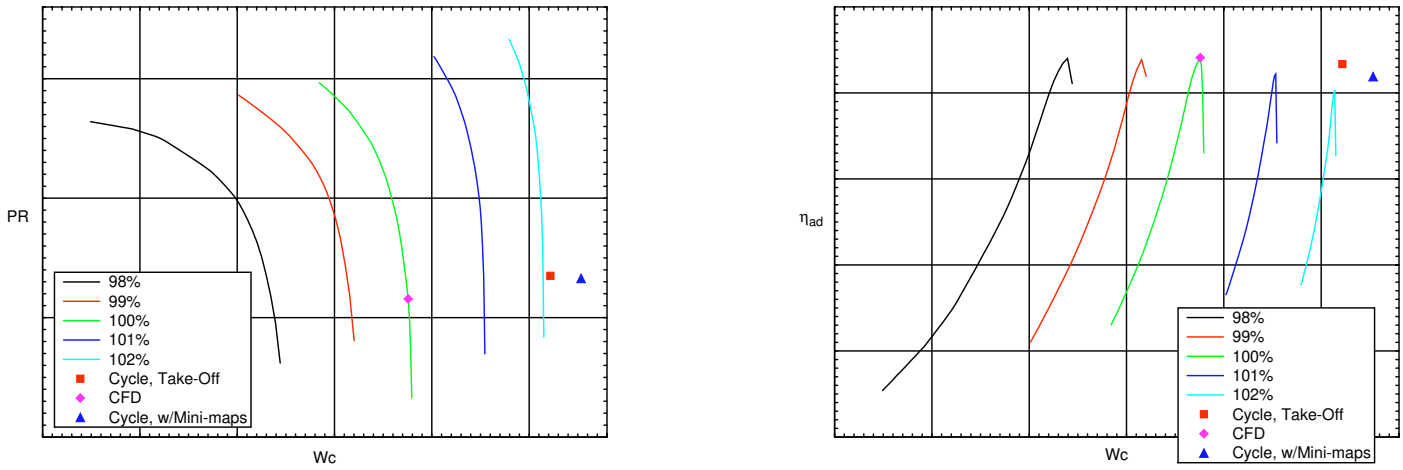

Figure 14. HPC mini-maps. Pressure-ratio (PR) and adiabatic efficiency (η_{ad}) as function of corrected mass flow rate for a set of speed lines.

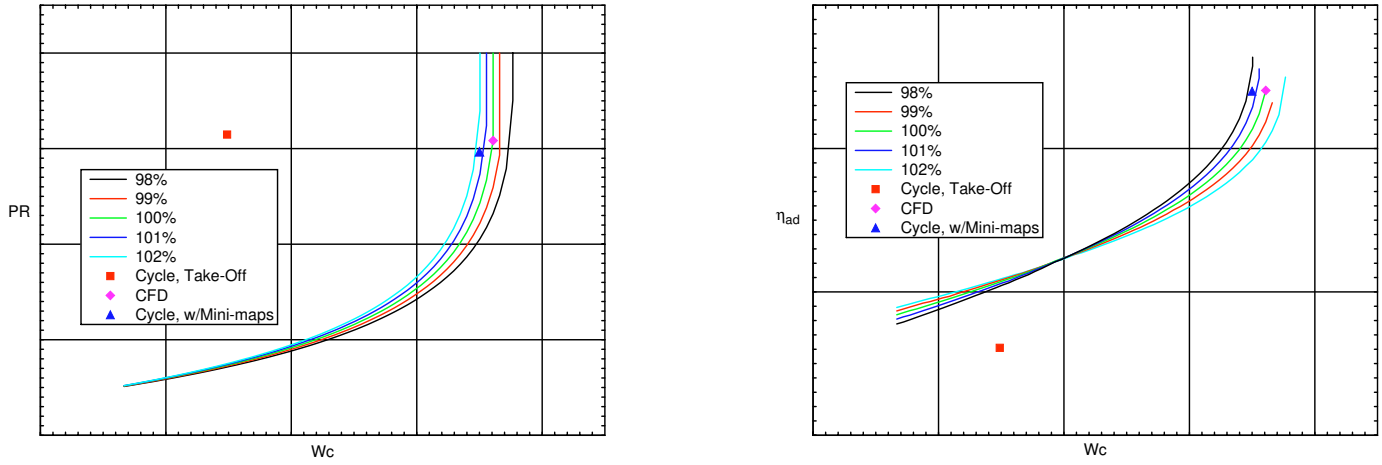

Figure 15. HPT mini-maps. Pressure-ratio (PR) and adiabatic efficiency (η_{ad}) as function of corrected mass flow rate (Wc) for a set of speed lines.

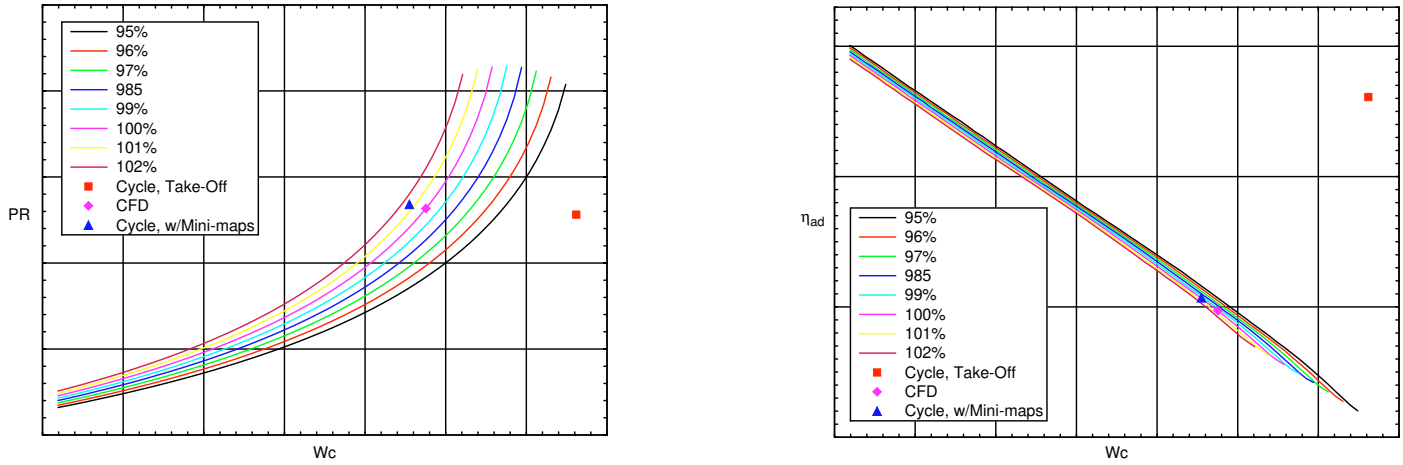

Figure 16. LPT mini-maps. Pressure-ratio (PR) and adiabatic efficiency (η_{ad}) as function of corrected mass flow rate (Wc) for a set of speed lines.

switch from the STGSTK method for the compression system to a modified form of the entropy-based blade row turbine model using NPSS appropriate for a compressor. The cycle model will also be modified to move the splitter downstream of the fan. NPSS would then be used for both zero-D and 1D modeling. Another advantage of using a blade row model is to understand the impact of global changes on a component in matching or flow capacity. This added understanding can then be used to tweak the 3D CFD to better align with expectations. For example by slightly changing the stagger angle of an IGV in the compressor or a turbine nozzle.

REFERENCES

[1] Reed. J. A., Turner, M. G., Norris, A., Veres, J. P., 2003, "Towards an Automated Full-Turbofan Engine Numerical Simulation," ISABE Paper No. 2003-1235.

[2] Lytle, J. K., 2000, "The Numerical Propulsion System Simulation: An Overview," NASA/TM-2000-209915.

[3] Lytle, J. K., 1994, "The Numerical Propulsion System Simulation: A Multidisciplinary design System For Aerospace Vehicles," NASA/TM-1999-209194.

[4] Smith, L. H., 1966, "The Radial-Equilibrium Equation of Turbomachinery," J. Eng. Gas Turb. Power, pp. 1-12.

[5] Adkins, G. G. and Smith, L. H., Jr., 1982, "Spanwise Mixing in Axial-Flow Turbomachines," J. Eng. Gas Turb. Power, 104(1), pp. 97-110.

[6] Adamczyk, J. J., 2000, "Aerodynamic Analysis of Multistage Turbomachinery Flows in Support of Aerodynamic Design," J. Turbomach., 122(2), pp. 189-217.

[7] Hall, E. J., 1997, "Aerodynamic Modeling of Multistage Compressor Flow Fields - Part 1: Analysis of Rotor/Stator/Rotor Aerodynamic Interaction," ASME Paper No. 97-GT-344.

[8] Hall, E. J., 1997, "Aerodynamic Modeling of Multistage Compressor Flow Fields - Part 2: Analysis of Rotor/Stator/Rotor Aerodynamic Interaction," ASME Paper No. 97-GT-345.

[9] Follen, G. J., and auBuchon, M., 2000, "Numerical Zooming between a NPSS Engine System Simulation and a 1-Dimensional High Compressor Analysis Code," NASA TM 2000-209913.

[10] E. J. Hall, R. A. Delaney, S. R. Lynn, and J. P. Veres, 1998, "Energy Efficient Engine Low Pressure Subsystem Aerodynamic Analysis," NASA/CR-1998-206402.

[11] Evans, A. L., Naiman, C. G., Lopez, I., and Follen, G. J., 1998, "Numerical Propulsion System Simulation's National Cycle Program", 34th AIAA/ASME/SAE/ASEE; Joint Propulsion Conference & Exhibit, Cleveland, OH, July 13-15.

[12] Liu, N. S. and Quealy, A., 1999, "A Multidisciplinary Design/Analysis Tool for Combustion," NASA CP1999-208757.

[13] Liu, N. S., 2001, "On the Comprehensive Modeling and Simulation of Combustion Systems," AIAA Paper No. 2001-0805, Reno, NV.

[14] Ryder, R. C., and McDivitt, T., 2000, "Application of the National Combustion Code Towards Industrial Gas Fired Heaters," AIAA Paper No. 2000-0456.

[15] Ebrahimi, H. B., Ryder, R. C., Brankovic, A., and Liu, N. S., 2001, "A Measurement Archive for Validation of the National Combustion Code", AIAA Paper No. 2001-0811.

[16] Adamczyk, J. J., Mulac, R. A., and Celestina, M. L., 1986, "A Model for Closing the Inviscid Form of the Average-Passage Equation System," J. Turbomach., 108, pp. 180-186.

[17] Kirtley, K. R., Turner, M. G., and Saeidi, S., 1999, "An Average Passage Closure Model for General Meshes," ASME Paper No. 99-GT-077.

[18] Turner, M. G., 2000, "Full 3D Analysis of the GE90 Turbofan Primary Flowpath", NASA/CR-2000-209951.

[19] Turner, M. G., Vitt, P. H, Topp, D., Saeidi, S., Hunter, S. D., Dailey, L.D. and Beach, T.A., 1999, "Multistage Simulations of the GE90 Turbine," ASME Paper No. 99-GT-98.

[20] Jameson, A. and Baker, T. J., 1984, "Multigrid Solutions of the Euler Equations for Aircraft Configurations," AIAA Paper No. 84-0093.

[21] Turner, M. G., and Jennions, I. K., 1993, "An Investigation of Turbulence Modeling in Transonic Fans Including a Novel Implementation of an Implicit k-e Turbulence Model," J. Turbomach., 115(2), pp. 249-260.

[22] Shabbir, A., Celestina, M.L., Adamczyk, J.J., and Strazisar, A.J., 1997, "The Effect of Hub Leakage Flow on Two High Speed Axial Flow Compressor Rotors," ASME Paper No. 97-GT-346.

[23] Steinke, R. J., 1982, "STGSTK: A Computer Code for Predicting Multistage Axial-Flow Compressor Performance by a Meanline Stage-Stacking Method," NASA TP 2020.

[24] Denton, J.D., 1993, "Loss Mechanisms in Turbomachines," J. Turbomach., 115(4), pp. 621-656.

[25] Lyman, F. A., 1993, "On the Conservation of Rothalpy in Turbomachines," J. Turbomach., 115(3), pp. 520-526.

[26] Turner, M. G., Ryder. R., Norris, A., Celestina, M., Moder, J., Liu, N. S., Adamczyk, J. and Veres, J., 2002, "High Fidelity 3D Turbofan Engine Simulation with Emphasis on Turbomachinery-Combustor Coupling," AIAA Paper No. 2002-3769.

[27] Portable Batch System External Reference Specification, 2000, James Patton Jones, ed., Veridian Systems, Inc.

[28] Turner, M. G., Norris, A. and Veres, J. P., 2003, "High Fidelity 3D Simulation of the GE90," AIAA 2002-3996, Orlando, FL.

[29] NASA-CR-174955 High Pressure Compressor (ICLS/10c) Compressor Performance Report Topical Report, Oct. 1983 - Jul. 1985 (General Electric Co.) 120 p X85-10387

[30] Plybon, R., 2003, GE Aircraft Engines, Personal Correspondence, Oct. 29, 2003

REPORT DOCUMENTATION PAGE

Form Approved
OMB No. 0704-0188

1. AGENCY USE ONLY (*Leave blank*)	2. REPORT DATE	3. REPORT TYPE AND DATES COVERED
	November 2004	Technical Memorandum

4. TITLE AND SUBTITLE

Multi-Fidelity Simulation of a Turbofan Engine With Results Zoomed Into Mini-Maps for a Zero-D Cycle Simulation

5. FUNDING NUMBERS

WBS–22–708–87–01

6. AUTHOR(S)

Mark G. Turner, John A. Reed, Robert Ryder, and Joseph P. Veres

7. PERFORMING ORGANIZATION NAME(S) AND ADDRESS(ES)

National Aeronautics and Space Administration
John H. Glenn Research Center at Lewis Field
Cleveland, Ohio 44135–3191

8. PERFORMING ORGANIZATION REPORT NUMBER

E–14551

9. SPONSORING/MONITORING AGENCY NAME(S) AND ADDRESS(ES)

National Aeronautics and Space Administration
Washington, DC 20546–0001

10. SPONSORING/MONITORING AGENCY REPORT NUMBER

NASA TM—2004-213076
GT2004–53956

11. SUPPLEMENTARY NOTES

Prepared for the Turbo Expo 2004 sponsored by the American Society of Mechanical Engineers Vienna, Austria, June 14–17, 2004. Mark G. Turner, University of Cincinnati, P.O. Box 210070, Cincinnati, Ohio 45221–0070; John A. Reed, AP Solutions, Inc., 5075 Everton Avenue, Solon, Ohio 44139; Robert Ryder, Flow Parametrics, LLC, 68 Bushy Hill Road, Ivoryton, Connecticut 06442; and Jospeh P. Veres, NASA Glenn Research Center. Responsible person, Joseph P. Veres, organization code 2900, 216–433–2436.

12a. DISTRIBUTION/AVAILABILITY STATEMENT

Unclassified - Unlimited
Subject Categories: 02, 34, and 07 Distribution: Nonstandard

Available electronically at http://gltrs.grc.nasa.gov

This publication is available from the NASA Center for AeroSpace Information, 301–621–0390.

12b. DISTRIBUTION CODE

13. ABSTRACT ***(Maximum 200 words)***

A Zero-D cycle simulation of the GE90-94B high bypass turbofan engine has been achieved utilizing mini-maps generated from a high-fidelity simulation. The simulation utilizes the Numerical Propulsion System Simulation (NPSS) thermodynamic cycle modeling system coupled to a high-fidelity full-engine model represented by a set of coupled 3D computational fluid dynamic (CFD) component models. Boundary conditions from the balanced, steady-state cycle model are used to define component boundary conditions in the full-engine model. Operating characteristics of the 3D component models are integrated into the cycle model via partial performance maps generated from the CFD flow solutions using one-dimensional meanline turbomachinery programs. This paper highlights the generation of the high-pressure compressor, booster, and fan partial performance maps, as well as turbine maps for the high pressure and low pressure turbine. These are actually "mini-maps" in the sense that they are developed only for a narrow operating range of the component. Results are compared between actual cycle data at a take-off condition and the comparable condition utilizing these mini-maps. The mini-maps are also presented with comparison to actual component data where possible.

14. SUBJECT TERMS

Gas turbine engine; Computational fluid dynamics; System simulation; Computer simulation

15. NUMBER OF PAGES

18

16. PRICE CODE

17. SECURITY CLASSIFICATION OF REPORT	18. SECURITY CLASSIFICATION OF THIS PAGE	19. SECURITY CLASSIFICATION OF ABSTRACT	20. LIMITATION OF ABSTRACT
Unclassified	Unclassified	Unclassified	